COMPDYN 2009
ECCOMAS Thematic Conference on
Computational Methods in Structural Dynamics and Earthquake Engineering
M. Papadrakakis, N.D. Lagaros, M. Fragiadakis (eds.)
Rhodes, Greece, 22–24 June 2009

TWO-DIMENSIONAL NUMERICAL MODELING OF LIGHT-FRAME WOOD STRUCTURES FOR SEISMIC COLLAPSE ASSESSMENT

Ioannis P. Christovasilis [1] **and Andre Filiatrault** [2]

Dept. of Civil, Structural and Environmental Engineering, University at Buffalo,
State University of New York, Buffalo, NY 14260, USA
email: [1] ipc@buffalo.edu, [2] af36@buffalo.edu

Keywords: Wood structures, Seismic analysis, Collapse assessment

Abstract. *The research work presented in this paper describes the numerical modeling of light-frame wood structures. This type of low-rise residential buildings is widely used across North America and incorporates sheathed woodframe shear walls as a lateral load-resisting system. The numerical model introduced attempts to address the dynamic response of two-dimensional woodframe buildings under unidirectional horizontal and vertical earthquake shaking, by effectively simulating the primary modes of deformation that have been observed and identified in recent three-dimensional shake table tests of a full-scale two-story light-frame wood townhouse building. A computer program is being developed that formulates a numerical two-dimensional building model at the nail level, yet maintains simplicity in the model preparation and can accommodate various structural configurations. The element library includes a number of nonlinear springs that capture the load-deformation characteristics of wood connections and vertical load-transferring devices up to complete failure, as well as contact/separation phenomena between framing members. A linear beam element is utilized for modeling the wood framing since the individual frame members do remain elastic and the nonlinear behavior is concentrated in the sheathing-to-framing and the framing-to-framing connections. A corotational formulation is employed to solve the equilibrium equations in the deformed configuration accounting for large rotations and large displacements associated with rigid body motion, geometric nonlinearity, as well as P-Δ effects at the system level. The preliminary analyses of one-story woodframe buildings indicate that the proposed model is capable of capturing more realistic load paths in the shear walls and the response is affected by their height-to-width ratio, the simulated gravity loads and the anchoring devices installed on the structure.*

1 INTRODUCTION

This paper describes a numerical investigation of the seismic response of light-frame wood structures. These low-rise residential buildings, widely used across North America, typically incorporate sheathed light-frame wood shear walls as lateral-load-resisting system. Since light-frame wood construction represents about 90% of the residential buildings in the United States and 99% of residences in California [1], a substantial portion of these structures is located in regions of moderate-to-high seismicity and is potentially susceptible to significant earthquake shaking during their life-spans.

1.1 Review of the seismic behavior of light-frame wood structures

Light-frame wood buildings consist of vertical (shear wall) and horizontal (floor) wood diaphragms. Figure 1a illustrates a single-story light-frame wood structure. Floor diaphragms distribute gravity and seismically induced loads to the wood shear walls and the seismic behavior of light-frame wood structures is dominated by the racking (shear) deformation of the shear walls along the horizontal directions parallel to the wall planes[1].

A wood shear wall, illustrated in Figure 1b, typically consists of (i) the framing members inter-connected with framing-to-framing connectors, (ii) the sheathing panels, and (iii) the sheathing-to-framing connectors (nails), typically distributed at a specified spacing along the panel edges. The in-plane lateral resistance is generated at the numerous sheathing-to-framing connections and the developed forces are directly related to the history of the displacement field of the connectors, defined as the difference between the deformations of the panel sheathing and the wood framing (Figs. 2a, 2b). It is the resultant connection forces acting on the wood framing that stabilizes the shear walls under the lateral loads transferred to the sill (bottom) and top plates from the floor diaphragms (Figs. 2c, 2d).

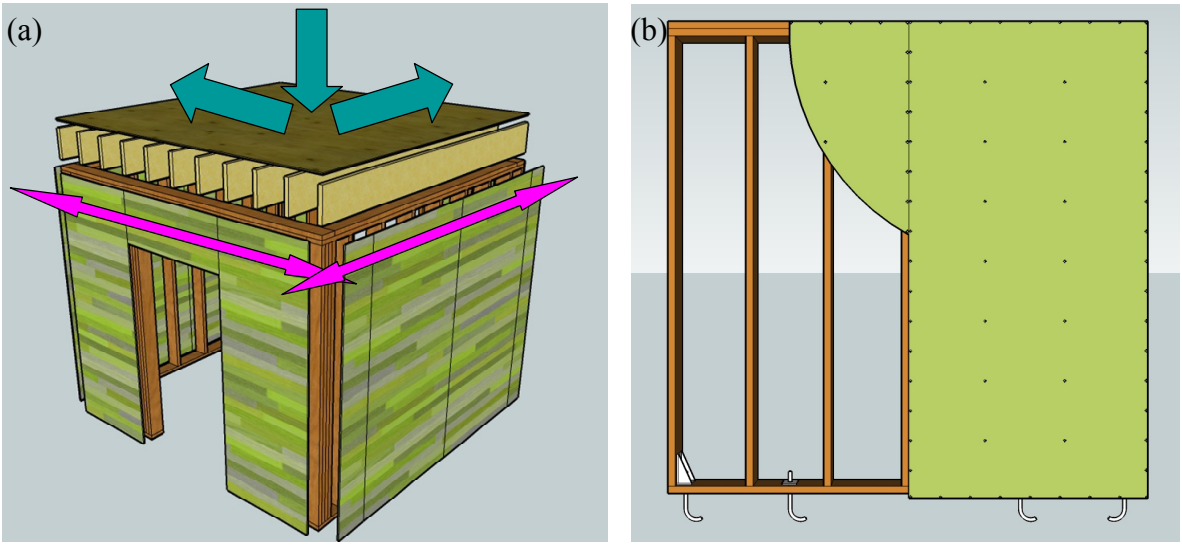

Figure 1: Illustration of (a) a single-story light-frame wood structure, and (b) a wood shear wall

The pure racking deformation of wood shear walls is associated with significant hysteretic damping and dissipated energy by the sheathing-to-framing connections. The force-displacement response of sheathing-to-framing connections, under cyclic loading, exhibits

[1] Typically, the lateral resistance of shear walls along the horizontal direction perpendicular to the wall plane is neglected in seismic design of light-frame wood buildings. The basic points provided in this discussion refer to force and displacement fields solely along the wall plane.

pinching characteristics as well as strength and stiffness degradation (Fig. 3a), while these characteristics can also be identified in the global response of wood shear walls (Fig. 3b). However, there are other modes of deformation, such as rocking or frictional sliding, that can affect the global lateral stiffness, strength, and energy dissipation characteristics of the inter-story wood walls, and subsequently modify the seismic response of the whole structure. The level of participation of secondary deformation modes other than pure racking kinematic distortion of the frame is related primarily to the load-deformation characteristics of the framing-to-framing connections as well as the shear-transferring and vertical load-anchoring devices between shear walls and floor diaphragms. Loads between framing members are transferred mainly through bearing and friction, but tensile forces that are developed under equilibrium to lateral forces and that overcome the gravity compressive loads may cause members to detach, exposing (i) the framing-to-framing connectors to tensile deformation fields (separation phenomena) coupled with shear-transferred loads, and (ii) the sheathing-to-framing connectors to modified displacement orbits to accommodate the local discontinuity of the wood framing. These phenomena modify the load paths from the structure to the ground and are associated in most cases with reduced global stiffness and energy dissipation capability.

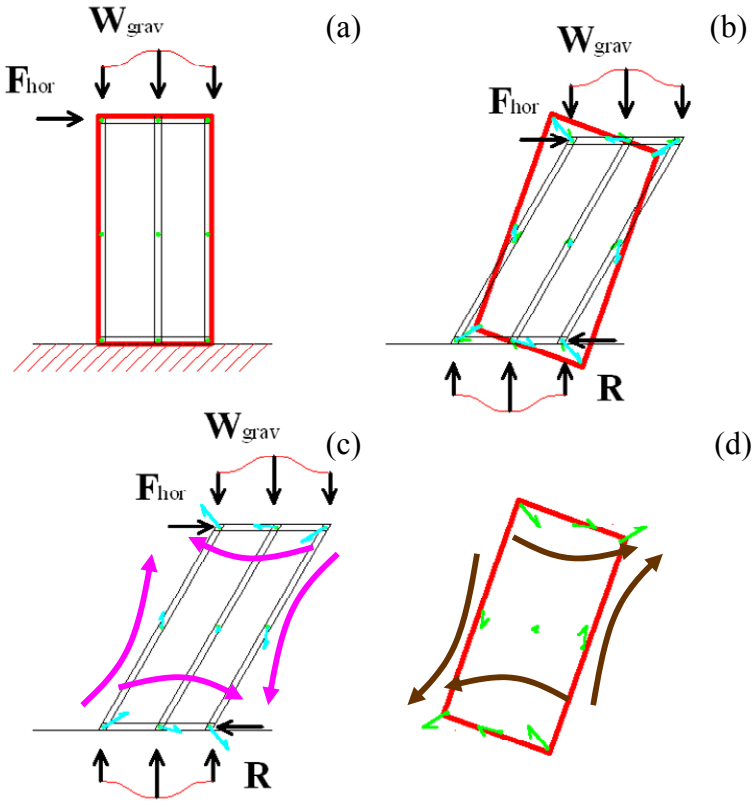

Figure 2: Deformation and free-body diagram of a single-panel shear wall under external loads

1.2 Damage of light-frame wood structures in past earthquakes

While light-frame wood buildings have historically performed well with regard to life safety requirements in regions of moderate-to-high seismicity, these types of low-rise structures have sustained significant structural and nonstructural damage in recent earthquakes.

Falk and Soltis [4], summarizing observations from damage of light-frame wood buildings from past earthquakes, reported the susceptibility to damage of (i) two-story and split-level homes with large garage openings and short wall piers at ground level (1971 San Fernando

Earthquake, Fig. 4a), and (ii) wood houses with short wood stud (cripple) walls in the substructure (1983 Coalinga and 1984 Halls Valley Earthquakes). Other observations from these three seismic events included failures at sill plate connections and homes shifting off foundations. The authors concluded that properly constructed light-frame wood buildings performed well, but indicated prophetically that, in the United States, little work had been conducted on improving the ductility capacity of wood structures.

Damage in light-frame wood buildings was also observed after the 1989 Loma Prieta Earthquake (Fig. 4b), but the 1994 Northridge Earthquake has been recognized as the seismic event that actually highlighted the seismic vulnerability of residential light-frame wood construction. It is indicative that out of the 25 fatalities caused by building damage during the Northridge Earthquake, 24 occurred in light-frame wood buildings [5]. Most of the fatalities were related to soft/first story collapse of apartment buildings with tuck-under garage and few to collapse of hillside houses inadequately supported on steep foundations [6]. Extensive damage in structural components and nonstructural wall finishes of light-frame wood buildings was the main contributor to the temporary displacement of 100,000 residents, which persisted as a long-term displacement of 50,000 residents [7]. The property loss to light-frame wood construction as a result of this single seismic event was estimated at $20 billion [8], and exceeded the loss to any other type of construction. Of the $12.3 billion paid out for insurance claims, 78% has been for residential claims, almost all of which was associated with light-frame wood construction [8].

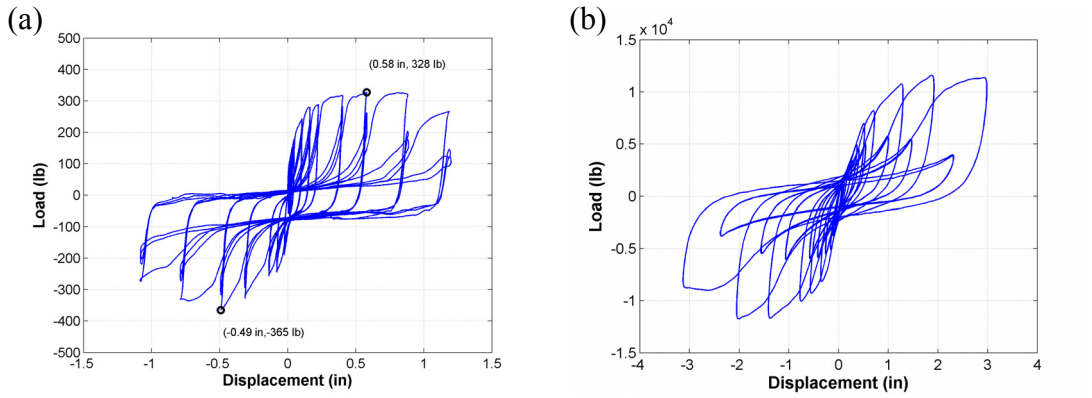

Figure 3: Qualitative demonstration of the cyclic response of (a) a sheathing-to-framing connection (after [2]), and (b) a light-frame wood shear wall (after [3])

Figure 4: (a) Collapse of a two-story building during San Fernando Earthquake due to inadequate lateral strength at the ground level. The tip of a crashed car reveals the existence of a garage opening with short wall piers. A similar adjacent building appears to be undisturbed, although diagonal cracking of the exterior wall finishes can be identified at the top left corner of the garage door, and (b) typical soft-story collapse of a residence during Loma Prieta Earthquake (photos credit: [9])

2 REVIEW ON MODELING OF LIGHT-FRAME WOOD BUILDINGS

The literature review provided in this section attempts to summarize and discuss some of the relevant published research contributions on the two-dimensional numerical analysis of light-frame wood structures under horizontal and vertical loads. Shear walls act as the primary lateral-load-resisting system in a light-frame wood structure and are traditionally designed under a force-based procedure that assumes a static horizontal force as a fraction of the tributary weight that is laterally supported by the wall. Construction guidelines or equilibrium-based engineering calculations can provide a capacity-based analysis of vertical load paths developed in the wood framing that can indicate the necessity for installation of (i) holdown devices in the end studs (vertical framing members) of the shear wall to resist uplifting inner forces, and (ii) anchor bolts in bottom sill plates in a specified spacing to transmit uplifting and lateral inner loads to the foundation, as shown in the illustration of a sample shear wall in Fig. 1b. While this design and construction practice leads to a building that can be conceptually – or performance-based – rated to have "superior design and construction quality", the majority of the residential houses in North America has been built with questionable and rather medium-to-poor construction quality [1]. With this point in mind, the review of available numerical models attempts to investigate and highlight the application of modeling techniques to describe the effects of vertical load paths and equally acknowledge the assumptions made in boundary conditions or inter-component connections.

Figure 5 illustrates the state-of-practice of dynamic response-history analysis using the 1st generation simplified wood shear wall models, which do not consider any other nonlinearity than the sheathing-to-framing connections [10]. These connections are represented by orthogonal pairs of nonlinear single-degree-of-freedom (SDOF) springs that are connected with the framing and the sheathing at the specified nail locations. The framing members are assumed to be rigid and pin-connected, the base is assumed to be fixed to the ground, while the sheathing panels are considered to deform in shear and translate and rotate in the wall plane as a rigid body. Under these assumptions, the static behavior of a shear wall can be captured by a SDOF nonlinear spring, the parameters of which are fitted to yield similar response to that obtained from the shear wall model (Figs. 5a, 5b). This procedure allows the use of a "pancake" building model [11, 12], in which the vertical dimension is suppressed and horizontal springs that connect rigid floor diaphragms represent one or a series of inter-story shear walls (Figs. 5c, 5d), achieving high computational efficiency[2]. Despite the simplified assumptions, these models have demonstrated good agreement with experimental results and have been used in reliability studies and recently in collapse analysis studies of light-frame wood structures [13, 14]. However, certain limitations have been also exposed due to the inability to predict the reduction in stiffness and strength of shear walls with high aspect (height-to-width) ratio and the neglection of second order P-Δ effects due to gravity loads.

More detailed finite element models have also been proposed that include framing flexibility, but simplified assumptions are considered for framing connections and boundary conditions [15, 16]. Typically, 2-noded beam and 4-noded (or 8-noded) shell elements are utilized

[2] Although the finite element static analysis of a single-panel shear wall can be executed fairly easily on a personal computer based on documented methods, when considering multi-panel shear walls across a single or multiple floors, the numerical solution poses a high computational overhead. Failure to meet these demands leads either to inability of the computer program to conclude the analysis or excessive time to facilitate the solution. The problem becomes more apparent when pursuing a dynamic response-history analysis, since this procedure requires a great number of solution steps for each earthquake record, and the seismic assessment usually involves the execution of multiple dynamic analyses with different ground motions. These reasons have led to the use of both detailed and simplified finite element models, depending on the physical size of the prototype and the type of analysis, favoring simplified modeling techniques, especially for dynamic analysis of 2D or 3D buildings.

within commercial finite element software to describe the framing and sheathing panels, respectively. The response obtained from such models will depend on the nonlinear behavior of the sheathing-to-framing connections and has been observed to be similar to what predicted by the simplified models [10], given that the connection constitutive models and properties are the same. Other studies have implemented more detailed modeling features, regarding (i) sheathing-to-framing connections [17], (ii) in-plane bearing between sheathing panels [18], and (iii) the effect of surrounding diaphragms in the response of wood shear walls [19-25].

However, the majority of the proposed finite element shear wall models are formulated on the basis of pinned framing-to-framing connections and fixed sill plate to the foundation. There are cases were linear or nonlinear connectors have been assigned between framing members but convenient "strict" boundary conditions are usually considered for the bottom or the top of shear walls or wall assemblies. There has been no numerical model, for cyclic or dynamic analysis, similar to that described in [23] for monotonic static analysis up to the ultimate force capacity, which (i) can incorporate separation of vertical studs from top and sill plates in conjunction with contact phenomena and anchoring devices in the direction normal to the adjacent horizontal diaphragms, and (ii) can allow separation and bending of the top and sill plate members. This type of coupled shear/bending/rocking structural response is usually suppressed in well anchored light-frame wood shear walls or walls with intermediate anchorage that carry a good portion of the total gravity loads. However, uplifting and rocking behavior has been experimentally observed especially in narrow shear walls with high aspect ratio [26-28] as well as in shake-table tests of full-scale light-frame wood structures [29, 30]. Two possible reasons for these omissions can be the numerical difficulty associated with modeling contact/separation conditions and the lack of experimental or analytical studies on the response of these types of connections, other than sheathing-to-framing connections.

Additionally, in all cases where commercial finite element software was employed for cyclic analysis of light-frame wood components, the researchers had to add in the element library additional user-defined hysteretic-spring elements, suitable for the main characteristics of wood connections. This reveals the complexity regarding finite element analysis of light-frame wood structures and explains why most research studies have focused on the development of in-house dedicated numerical models.

The numerical model proposed herein will focus on the modeling of framing and anchoring connections as well as on the simulation of appropriate boundary conditions. In order to do so, 2-noded beam elements shall be used to mesh the framing members, while sheathing panels shall be described through generalized displacement fields, similar to 1st generation models. This choice has been made acknowledging that meshing of the sheathing panels does not offer much higher accuracy if linear response is considered, yet increases substantially the required kinematic degrees-of-freedom (DOF) and consequently the computational overhead.

3 RESEARCH MOTIVATION

Summarizing the reasons that have motivated the research study described in this paper, these are:

i. The inability of 1st generation simplified numerical models to predict the differences in the lateral response of light-frame wood shear walls of identical nailing schedule but varying aspect ratio;
ii. The lack of documented finite element numerical models to predict the differences in the lateral response of light-frame wood shear walls with various anchorage conditions at the base;
iii. The lack of computationally efficient numerical models of light-frame wood shear walls with detailed modeling features.

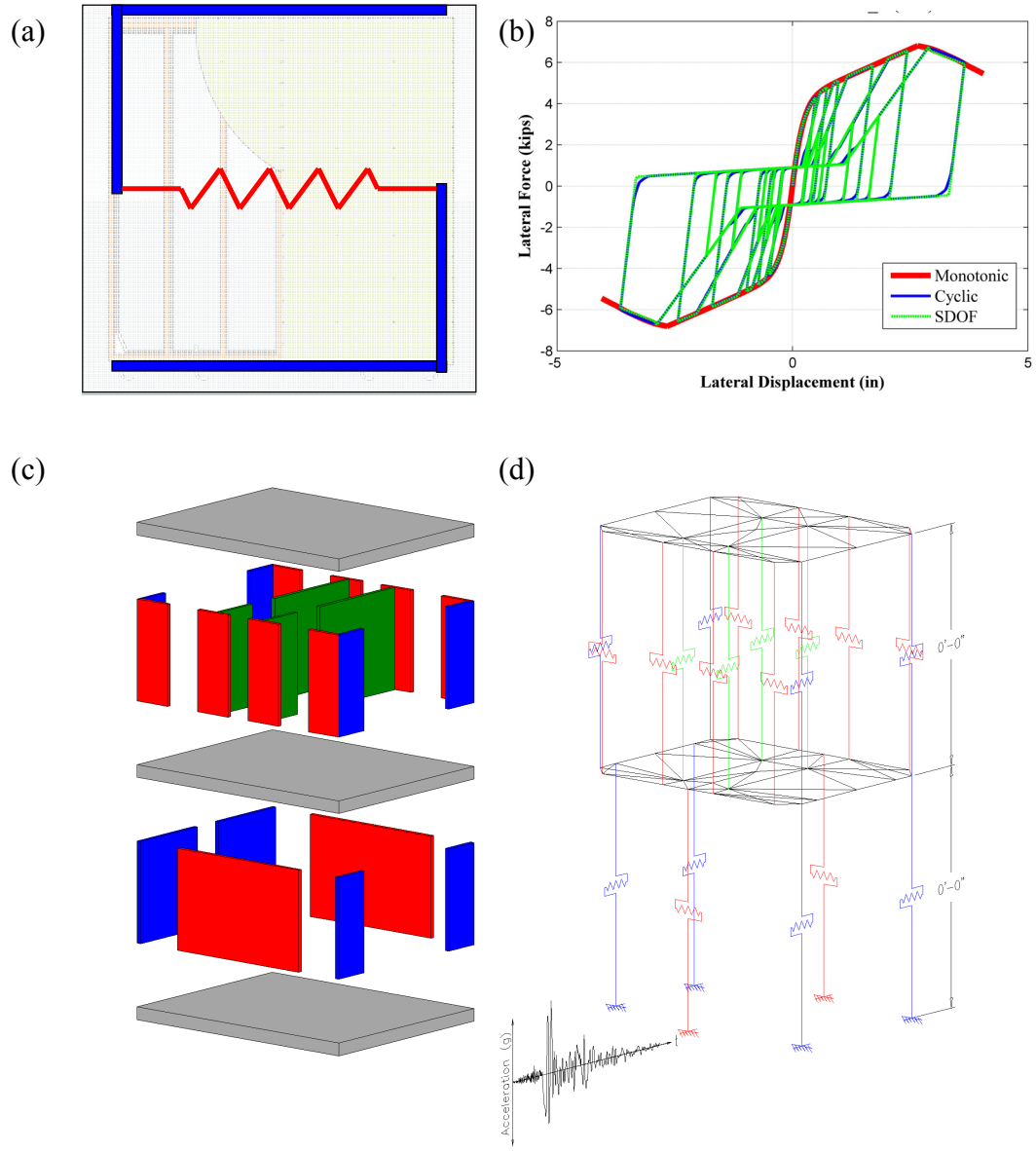

Figure 5: Modeling of light-frame wood buildings with 1st generation simplified models, CASHEW [10] and SAWS [11, 12], (a) equivalent SDOF spring of a wood shear wall, (b) fitting of SDOF spring parameters to match the cyclic response of the wall assembly, (c) building sketch of a two-story light-frame wood structure, and (d) equivalent "pancake" building model (after [29])

3.1 Experimental study

As part of the NSF/NEES-funded NEESWood Project: "Developing Performance-Based Seismic Design Philosophy for Mid-Rise Woodframe Construction," an experimental program that involved the three-dimensional shake-table testing of a full-scale two-story light-frame wood townhouse building was conducted at the University at Buffalo. The test structure, designed and constructed according to applicable practices in the 80's or 90's in California, represented one of the largest building specimens ever tested under three-dimensional earthquake simulation and utilized both twin shake tables at the Structural Engineering and Earthquake Simulation Laboratory (SEESL) at the University at Buffalo. The 9-month experimental program, incorporating 5 test phases associated with different structural configurations of the building, was selected as such to provide a wide set of recorded data that can enable observation, identification and quantification of fundamental aspects that affect the

seismic performance of a light-frame wood building with realistic dimensions, under increased levels – beyond design-basis – of shaking. The qualitative and quantitative observations from the benchmark test results can be directly applicable to performance-based design and analysis procedures, conducted within the NEESWood Project. The testing procedures and the main results of the processed data have been documented in [30]. The conclusion of this two-phase study, related to the experimental task and the meta-data-analysis task, has provided important guidance on the development of the proposed numerical model.

Figures 6a and 6b show photographs of the test structure during the first and last test phase of the experimental program, respectively. Figure 6c depicts the peak vertical displacements of the sill plate and the local stud for various walls of the 1st floor of the test structure. Similarly, Figure 6d depicts the peak forces developed at the anchor bolts and holdown devices installed at the base of the 1st floor shear walls. These data has been recorded during a tri-axial seismic input motion – unscaled Rinaldi ground motion from the 1994 Northridge Earthquake – that represented a seismic level similar to the Maximum Considered Earthquake (MCE) level of shaking. These results demonstrate qualitatively that nonlinear wall boundary conditions do exist (sill plate uplift/separation from the ground) as well as internal nonlinear deformations in the framing (separation of studs from sill plate). Uplift displacements are higher in wall assemblies without holdowns at the end studs, and similarly the high uplifting forces developed at the holdowns reveal that end studs without holdowns will be prone to separate from the sill plate.

4 MODEL FORMULATION

This section presents the numerical framework employed to solve the nonlinear static equilibrium equations of a single-story light-frame wood shear wall with multiple sheathing panels, under any combination of prescribed displacement and/or force histories applied in the wall plane. This is the first and most important step towards the dynamic response-history analysis of two-dimensional single- or multi-story buildings for two reasons. First, the aforementioned framework will result in a shear wall element, to be used for each story of a dynamic building model. Secondly, succeeding to solve the nonlinear static equilibrium equations, within a multi-step iterative procedure, at all possible displacement fields of interest – in this case, up to complete failure/collapse of the lateral-load-resisting system – ensures success in the solution of the dynamic equilibrium equations too. During a dynamic solution framework not only the incremental solution time-steps are typically bounded to small values to meet certain numerical stability and accuracy requirements, but also the dynamic tangent stiffness matrix inverted during the iterative solution process is in almost all cases positive definite even if the tangent stiffness matrix becomes non positive definite.

Before introducing the finite elements formulated and utilized in this study, it should be noted that the objective is to satisfy the equilibrium equations in the deformed configuration, accounting for large displacements, associated with large rotations, and consequently P-Δ effects at the system level. This procedure requires an iterative solution procedure even if the elements remain elastic, due to the associated geometric nonlinearity.

4.1 Frame element

The basic component of the two-dimensional model consists of the frame elements representing the wood framing. The frame element is the well-known 2-noded beam element with 3 DOF per node (two translations and one rotation). It is assumed that each element has flexural and axial rigidity **EI** and **EA**, respectively, and an initial length $\mathbf{L_0}$. The element has elastic material properties, assuming small deformations that do not change the constitutive model.

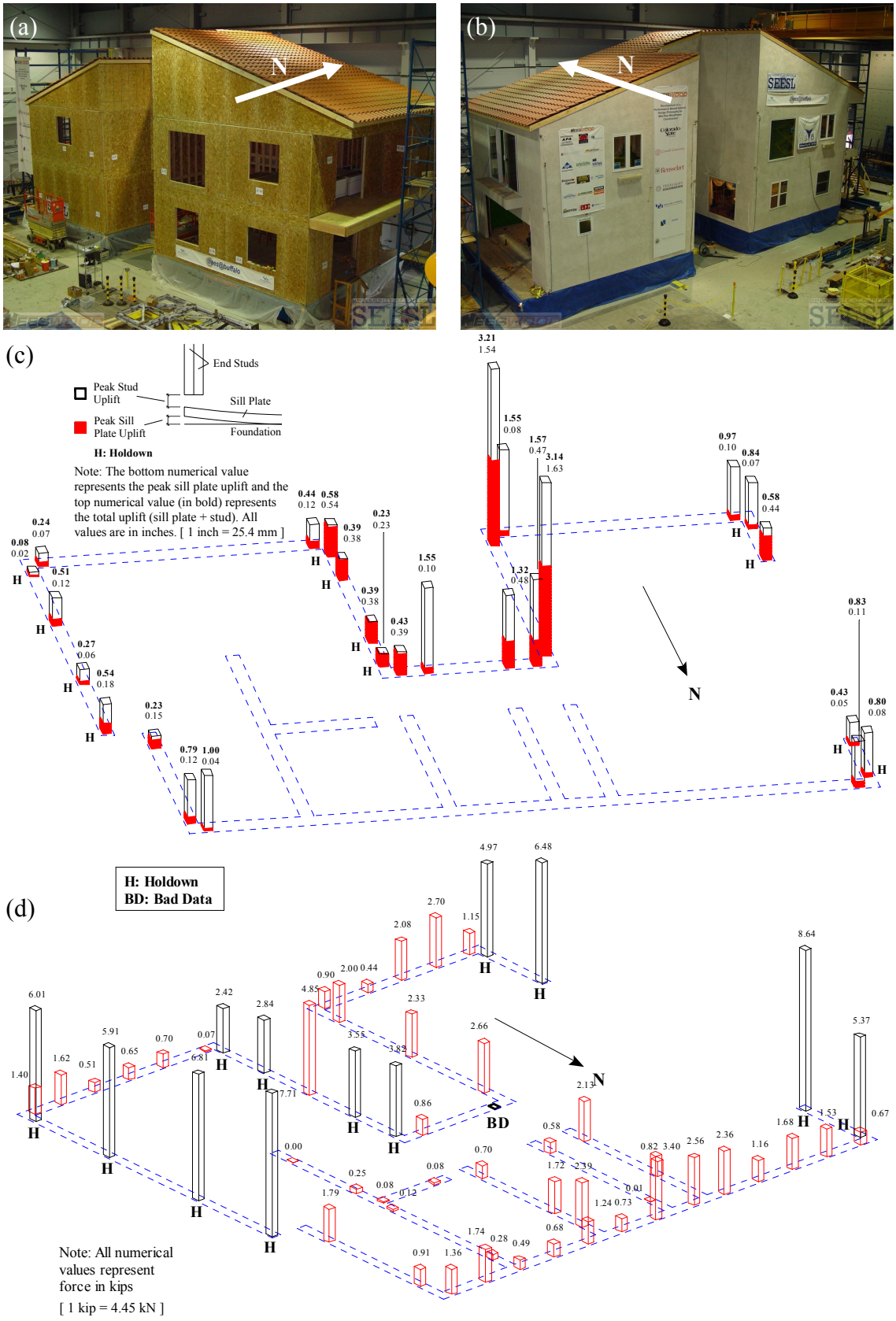

Figure 6: University at Buffalo NEESWood benchmark tests, (a) south-east view of the test structure featuring only the structural wood shear walls, (b) south-west view of the test structure featuring the structural wood shear walls and the non-structural wall finishes, (c) peak sill plate and stud uplift for MCE level tri-axial seismic motion, and (d) peak anchor bolt and holdown forces for MCE level tri-axial seismic motion (after [30])

If we derive the equilibrium equations in a Local Coordinate System (LCS) with the x axis crossing through the nodes, as shown in Figure 7a, there are only 3 local deformation DOF, 1 axial elongation **u** and 2 rotations of the nodes $\mathbf{z_1}$ and $\mathbf{z_2}$ [31]. The equilibrium equations relating the axial force **f** and the two moments at the nodes $\mathbf{m_1}$ and $\mathbf{m_2}$ with the local DOF are:

$$\begin{Bmatrix} \mathbf{f} \\ \mathbf{m}_1 \\ \mathbf{m}_2 \end{Bmatrix}_{\mathbf{L}} = \left[\mathbf{k}_f\right] \cdot \begin{Bmatrix} \mathbf{u} \\ \mathbf{z}_1 \\ \mathbf{z}_2 \end{Bmatrix}_{\mathbf{L}} \Rightarrow \begin{Bmatrix} \mathbf{f} \\ \mathbf{m}_1 \\ \mathbf{m}_2 \end{Bmatrix}_{\mathbf{L}} = \begin{bmatrix} \mathbf{EA}/\mathbf{L_0} & 0 & 0 \\ 0 & 4.\mathbf{EI}/\mathbf{L_0} & 2.\mathbf{EI}/\mathbf{L_0} \\ 0 & 2.\mathbf{EI}/\mathbf{L_0} & 4.\mathbf{EI}/\mathbf{L_0} \end{bmatrix} \cdot \begin{Bmatrix} \mathbf{u} \\ \mathbf{z}_1 \\ \mathbf{z}_2 \end{Bmatrix}_{\mathbf{L}} \tag{1}$$

In this corotational formulation the local stiffness matrix [$\mathbf{k}_f$] remains constant and depends only on the elastic properties and the initial length of the element. The transverse forces in the LCS are calculated through equilibrium with the bending moments, based on the actual length **L** of each element at the current solution step. The element force vector $\{\mathbf{f_L}\}$ in the LCS is:

$$\{\mathbf{f}_\mathbf{L}\} = \left[\mathbf{N(L)}\right]^\mathbf{T} \cdot \begin{Bmatrix} \mathbf{f} \\ \mathbf{m}_1 \\ \mathbf{m}_2 \end{Bmatrix}_{\mathbf{L}} \Rightarrow \{\mathbf{f}_\mathbf{L}\} = \begin{bmatrix} -1 & 0 & 0 \\ 0 & 1/\mathbf{L} & 1/\mathbf{L} \\ 0 & 1 & 0 \\ 1 & 0 & 0 \\ 0 & -1/\mathbf{L} & -1/\mathbf{L} \\ 0 & 0 & 1 \end{bmatrix} \cdot \begin{Bmatrix} \mathbf{f} \\ \mathbf{m}_1 \\ \mathbf{m}_2 \end{Bmatrix}_{\mathbf{L}} \tag{2}$$

The global force vector $\{\mathbf{f_G}\}$ for a given angle $\mathbf{\Phi}$ is:

$$\{\mathbf{f}_\mathbf{G}\} = \begin{bmatrix} \Lambda_f(\mathbf{\Phi})^\mathbf{T} & [\mathbf{0}] \\ [\mathbf{0}] & \Lambda_f(\mathbf{\Phi})^\mathbf{T} \end{bmatrix} \cdot \{\mathbf{f}_\mathbf{L}\} \tag{3}$$

$$\text{where } \left[\Lambda_f(\mathbf{\Phi})\right]^\mathbf{T} = \begin{bmatrix} \cos(\mathbf{\Phi}) & -\sin(\mathbf{\Phi}) & 0 \\ \sin(\mathbf{\Phi}) & \cos(\mathbf{\Phi}) & 0 \\ 0 & 0 & 1 \end{bmatrix} \tag{4}$$

The global stiffness matrix of a frame element [$\mathbf{K}_f$] is:

$$\left[\mathbf{K}_f\right] = \begin{bmatrix} \Lambda_f(\mathbf{\Phi})^\mathbf{T} & [\mathbf{0}] \\ [\mathbf{0}] & \Lambda_f(\mathbf{\Phi})^\mathbf{T} \end{bmatrix} \cdot \left[\mathbf{N(L)}\right]^\mathbf{T} \cdot \left[\mathbf{k}_f\right] \cdot \left[\mathbf{N(L)}\right] \cdot \begin{bmatrix} \Lambda_f(\mathbf{\Phi}) & [\mathbf{0}] \\ [\mathbf{0}] & \Lambda_f(\mathbf{\Phi}) \end{bmatrix} \tag{5}$$

In order to calculate and update the global internal force vector, the internal (local) deformations of the element $\{\mathbf{u}\ \mathbf{z_1}\ \mathbf{z_2}\}_\mathbf{L}^\mathbf{T}$ must be found first based on the updated displacement vector $\{\mathbf{u_1}\ \mathbf{v_1}\ \mathbf{z_1}\ \mathbf{u_2}\ \mathbf{v_2}\ \mathbf{z_2}\}^\mathbf{T}$ for each element. The new length of the element **L** is (Fig. 7b):

$$\mathbf{L} = \left\| \begin{Bmatrix} \mathbf{x}_2 - \mathbf{x}_1 + \mathbf{u}_2 - \mathbf{u}_1 \\ \mathbf{y}_2 - \mathbf{y}_1 + \mathbf{v}_2 - \mathbf{v}_1 \end{Bmatrix} \right\| = \left\| \begin{Bmatrix} \Delta\mathbf{x} + \Delta\mathbf{u} \\ \Delta\mathbf{y} + \Delta\mathbf{v} \end{Bmatrix} \right\| = \sqrt{\Delta\mathbf{x}^2 + \Delta\mathbf{y}^2 + \Delta\mathbf{u}^2 + \Delta\mathbf{v}^2} \tag{6}$$

where $(\mathbf{x_1},\mathbf{y_1})$ and $(\mathbf{x_2},\mathbf{y_2})$ are the global coordinates of the two nodes of the frame element. The new angle $\mathbf{\Phi}$ can be calculated from the initial angle $\mathbf{\Phi_0}$ as shown in (7), while the internal deformations based on the global deformations shown in Fig. 8b are computed in (8).

$$\Phi = \Phi_0 + d\Phi = \Phi_0 + \arcsin\left(\frac{\Delta x \cdot \Delta v - \Delta y \cdot \Delta u}{L \cdot L_0}\right) \tag{7}$$

$$\{u \quad z_1 \quad z_2\}_L^T = \left\{\left(L^2 - L_0^2\right)/\left(L + L_0\right) \quad \left(z_1 - d\Phi\right) \quad \left(z_2 - d\Phi\right)\right\}^T \tag{8}$$

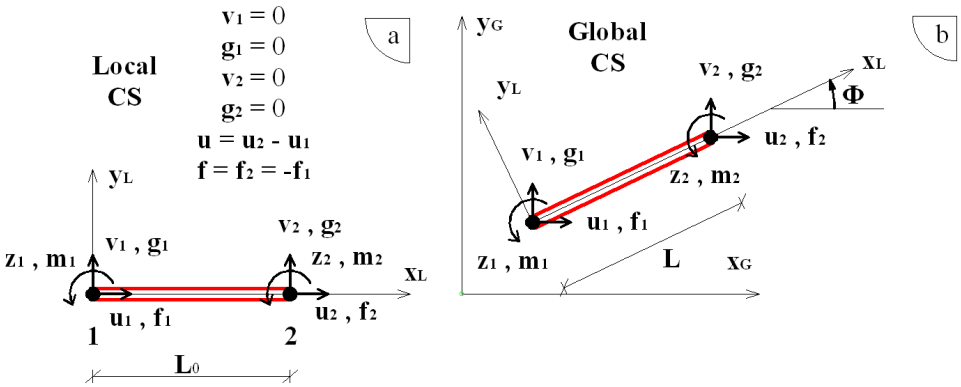

Figure 7: Kinematics of a frame element (a) in the Local CS, and (b) in the Global CS

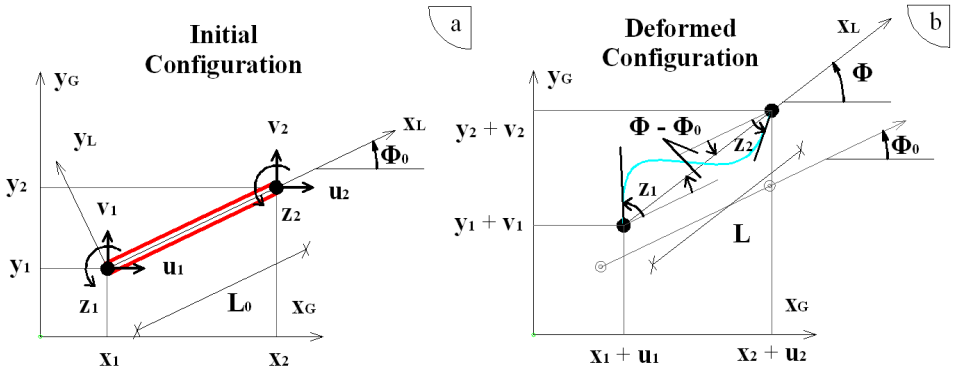

Figure 8: (a) Initial and (b) deformed configuration of a frame element

4.2 Panel element with sheathing-to-framing connectors

Each rectangular panel is modeled with a single panel element that also contains the sheathing-to-framing connectors. The latter connectors can be considered to be internal members of the system that connect the sheathing and the framing at discrete points, which initially coincide in the wall plane. The displacement field of the panel sheathing is described through 4 generalized DOF, 3 rigid body DOF (**U**, **V** and **Θ**) and 1 shear deformation ($\mathbf{U}_\gamma$), as shown in Figure 9. The displacement vector of each point in the panel $\{\mathbf{u_i}\}$, located in $\{\mathbf{X_i}\} = \{\mathbf{x_i}\ \mathbf{y_i}\}^T$, is calculated based on the panel element displacement vector $\{\mathbf{U_P}\} = \{\mathbf{U}\ \mathbf{V}\ \mathbf{\Theta}\ \mathbf{U}_\gamma\}^T$.

$$\{\mathbf{u_i}\} = f\left(\{\mathbf{U_P}\}\right) = \begin{Bmatrix}\mathbf{U}\\ \mathbf{V}\end{Bmatrix} + \begin{bmatrix}\cos\Theta & -\sin\Theta\\ \sin\Theta & \cos\Theta\end{bmatrix} \cdot \left(\{\mathbf{X_i}\} + \{\mathbf{u_i}\}_\gamma\right) - \{\mathbf{X_i}\} \tag{9}$$

where $\{\mathbf{u_i}\}_\gamma$ is the point displacement vector associated with the shear panel deformation and **h** is the height of the panel. Note that $\{\mathbf{X_i}\}$ refers to a LCS (origin at the panel center).

$$\{\mathbf{u_i}\}_\gamma = \begin{bmatrix}\mathbf{y_i/h}\\ \mathbf{0}\end{bmatrix} \cdot \mathbf{U}_\gamma \tag{10}$$

The four equilibrium equations, associated with each panel are expressed based on the point force vector $\{\mathbf{f_i}\}$ developed at each of the **n** sheathing-to-framing connections (see Fig. 10). The panel element force vector $\{\mathbf{F_P}\} = \{\mathbf{F_x\ F_y\ M\ T}\}^{\mathbf{T}}$ is calculated as:

$$\begin{Bmatrix} \mathbf{F_x} \\ \mathbf{F_y} \\ \mathbf{M} \\ \mathbf{T} \end{Bmatrix} = \begin{bmatrix} 1 & 0 & \dots & 1 & 0 & \dots & 1 & 0 \\ 0 & 1 & \dots & 0 & 1 & \dots & 0 & 1 \\ \{-\mathbf{y_1} & \mathbf{x_1}\}_{\Theta,\gamma} & \dots & \{-\mathbf{y_i} & \mathbf{x_i}\}_{\Theta,\gamma} & \dots & \{-\mathbf{y_n} & \mathbf{x_n}\}_{\Theta,\gamma} \\ \frac{\mathbf{y_1}}{\mathbf{h}}\cdot\{\cos\Theta & \sin\Theta\} & \dots & \frac{\mathbf{y_i}}{\mathbf{h}}\cdot\{\cos\Theta & \sin\Theta\} & \dots & \frac{\mathbf{y_n}}{\mathbf{h}}\cdot\{\cos\Theta & \sin\Theta\} \end{bmatrix} \cdot \begin{Bmatrix} \mathbf{f_{x,1}} \\ \mathbf{f_{y,1}} \\ . \\ \mathbf{f_{x,i}} \\ \mathbf{f_{y,i}} \\ . \\ \mathbf{f_{x,n}} \\ \mathbf{f_{y,n}} \end{Bmatrix} = \begin{Bmatrix} 0 \\ 0 \\ 0 \\ \mathbf{K_G}\cdot\mathbf{U_\gamma} \end{Bmatrix}$$

$$\Rightarrow \begin{Bmatrix} \mathbf{F_x} \\ \mathbf{F_y} \\ \mathbf{M} \\ \mathbf{T} \end{Bmatrix} = \sum_{\mathbf{i=1..n}} \left(\begin{bmatrix} 1 & 0 & \{-\mathbf{y_i}\}_{\Theta,\gamma} & \frac{\mathbf{y_i}}{\mathbf{h}}\cdot\cos\Theta \\ 0 & 1 & \{\mathbf{x_i}\}_{\Theta,\gamma} & \frac{\mathbf{y_i}}{\mathbf{h}}\cdot\sin\Theta \end{bmatrix}^{\mathbf{T}} \cdot \begin{Bmatrix} \mathbf{f_{x,i}} \\ \mathbf{f_{y,i}} \end{Bmatrix} \right) = \begin{Bmatrix} 0 \\ 0 \\ 0 \\ \mathbf{K_G}\cdot\mathbf{U_\gamma} \end{Bmatrix} \Rightarrow$$

$$\{\mathbf{F_P}\} = \sum_{\mathbf{i=1..n}} \left([\mathbf{A_i}]^{\mathbf{T}} \cdot \{\mathbf{f_i}\} \right) = \{0\ 0\ 0\ \mathbf{K_G}\cdot\mathbf{U_\gamma}\}^{\mathbf{T}} \tag{11}$$

$$\text{where } \mathbf{K_G} = \mathbf{G}\cdot\frac{\mathbf{b}\cdot\mathbf{t}}{\mathbf{h}} \tag{12}$$

$$\{\mathbf{X_i}\}_{\Theta,\gamma} = \{\mathbf{x_i}\quad \mathbf{y_i}\}^{\mathbf{T}}_{\Theta,\gamma} = \{\mathbf{X_i}\} + \{\mathbf{u_i}\}_{\Theta,\gamma} \overset{(9)}{=} \{\mathbf{X_i}\} + \left(\{\mathbf{u_i}\} - \{\mathbf{U\ V}\}^{\mathbf{T}}\right) \tag{13}$$

and **G** is the shear modulus, **b** is the width and **t** the thickness of the sheathing panel.

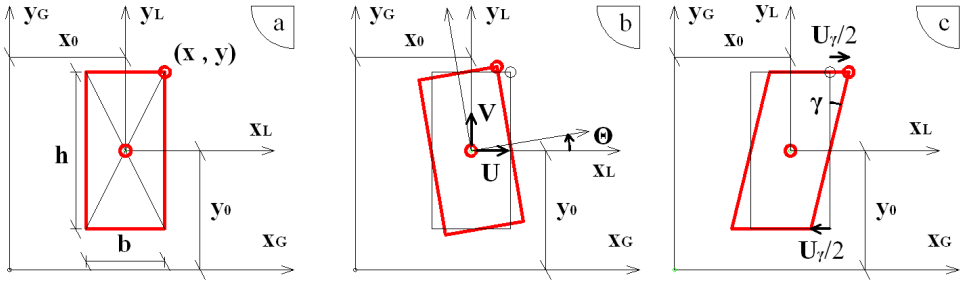

Figure 9: (a) Geometric configuration, (b) kinematic DOF associated with rigid body motion, and (c) shear mode of deformation of a panel element

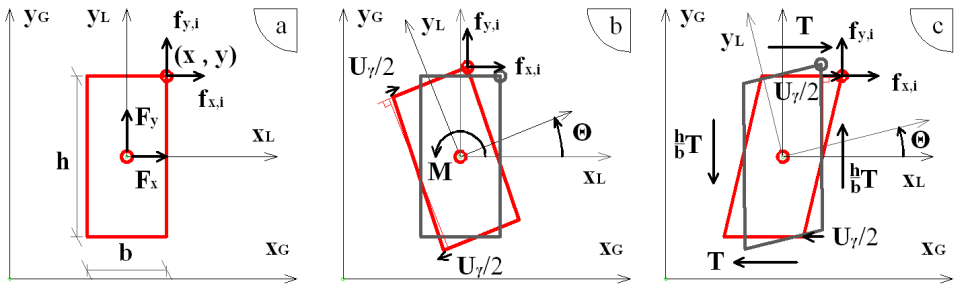

Figure 10: Generalized (a) global orthogonal forces, (b) moment, and (c) shear actions of a panel element

Each sheathing-to-framing connector consists of two orthogonal nonlinear springs, the 4x4 stiffness matrix $[\mathbf{K}_{C,i}]$ of which can be defined as:

$$\left[\mathbf{K}_{C,i}\right] = \begin{bmatrix} \left[\mathbf{k}_{con,i}\right] & -\left[\mathbf{k}_{con,i}\right] \\ -\left[\mathbf{k}_{con,i}\right] & \left[\mathbf{k}_{con,i}\right] \end{bmatrix}$$
$$\left[\mathbf{k}_{con,i}\right] = \begin{bmatrix} \mathbf{k}_{x,i} & \mathbf{k}_{xy,i} \\ \mathbf{k}_{yx,i} & \mathbf{k}_{y,i} \end{bmatrix} \tag{14}$$

where $\mathbf{k}_x$, $\mathbf{k}_y$ and $\mathbf{k}_{xy}$ are the stiffnesses of the connector **i**, in the Global Coordinate System (GCS). The connector force in (11) can be expressed as:

$$\{\mathbf{f}_i\} = \left[\mathbf{k}_{con,i}\right]\cdot\left(\{\mathbf{u}_{f,i}\} - \{\mathbf{u}_{p,i}\}\right) = \left[\mathbf{k}_{con,i}\right]\cdot\left(\{\mathbf{u}_{f,i}\} - \left[\mathbf{A}_i\right]\cdot\{\mathbf{U}_P\}\right) \tag{15}$$

In (15), it is assumed that $\{\mathbf{u}_{p,i}\} = [\mathbf{A}_i]\cdot\{\mathbf{U}_p\}$. This assumption holds incrementally and is the linearized version of the exact nonlinear relationship presented in (9).

The equilibrium equations of a sample shear wall can be written in the following format:

$$\begin{Bmatrix} \mathbf{F}_F \\ \mathbf{F}_P \end{Bmatrix} = \begin{bmatrix} \left[\mathbf{K}_{FF}\right] & \left[\mathbf{K}_{FP}\right] \\ \left[\mathbf{K}_{PF}\right] & \left[\mathbf{K}_{PP}\right] \end{bmatrix}\cdot\begin{Bmatrix} \mathbf{U}_F \\ \mathbf{U}_P \end{Bmatrix} \tag{16}$$

where the stiffness matrices in (16) are defined as:

$$\left[\mathbf{K}_{FF}\right] = \begin{bmatrix} \left[\mathbf{k}_{con,1}\right] & \dots & \left[\mathbf{0}\right] & \dots & \left[\mathbf{0}\right] \\ \dots & \dots & \dots & \dots & \dots \\ \left[\mathbf{0}\right] & \dots & \left[\mathbf{k}_{con,i}\right] & \dots & \left[\mathbf{0}\right] \\ \dots & \dots & \dots & \dots & \dots \\ \left[\mathbf{0}\right] & \dots & \left[\mathbf{0}\right] & \dots & \left[\mathbf{k}_{con,n}\right] \end{bmatrix} \qquad \left[\mathbf{K}_{FP}\right] = -\begin{bmatrix} \left[\mathbf{k}_{con,1}\right]\cdot\left[\mathbf{A}_1\right] \\ \dots\dots\dots\dots \\ \left[\mathbf{k}_{con,i}\right]\cdot\left[\mathbf{A}_i\right] \\ \dots\dots\dots\dots \\ \left[\mathbf{k}_{con,n}\right]\cdot\left[\mathbf{A}_n\right] \end{bmatrix}$$
$$\left[\mathbf{K}_{PF}\right] = \left[\mathbf{K}_{FP}\right]^T \qquad \left[\mathbf{K}_{PP}\right] = \begin{bmatrix} 0 & 0 & 0 & 0 \\ 0 & 0 & 0 & 0 \\ 0 & 0 & 0 & 0 \\ 0 & 0 & 0 & \mathbf{K}_G \end{bmatrix} + \begin{bmatrix} \\ \sum_{i=1..n}\left(\left[\mathbf{A}_i\right]^T\cdot\left[\mathbf{k}_{con,i}\right]\cdot\left[\mathbf{A}_i\right]\right) \\ \\ \end{bmatrix} \tag{17}$$

4.3 Modeling of sheathing-to-framing connections

The sheathing-to-framing connections are the only nonlinear inelastic elements used in this numerical model. Typically, a pair of orthogonal springs that connect the horizontal and vertical translational DOF of the frame and the panel at each connection point has been utilized in most of the proposed models (Fig. 11b). It has been recognized, however, that the use of two independent springs tends to over-estimate the stiffness and strength of the connection. Intuitively, the use of a single spring is more appropriate (Fig. 11a), but instability under cyclic loading eliminates this option. Studies presented in [16, 32] have demonstrated that the orientation of the pair of orthogonal springs, according to the first trajectory of the orbit (Fig. 11c), produces more reasonable results, eliminating the over-estimation of stiffness and strength. However, if gravity loads are applied in the first phase of the analysis, then the first trajectory

of each sheathing-to-framing connection coincides with the vertical direction. For this reason, in this study, a pair of orthogonal springs oriented initially with the GCS has been used. Additionally, the orthogonal springs rotate rigidly with the associated frame node, satisfying the primary objective of expressing equilibrium equations in the deformed configuration.

The constitutive model for each SDOF nonlinear spring has been presented in [33], although different constitutive models can be easily implemented as a subroutine that inputs a displacement history and outputs the associated force history as well as the tangent stiffness at each step. The hysteretic model proposed in [33] features an evolution of the model parameters, based on various damage indices, and a smooth force-displacement response, typical of wood connections, during loading, unloading and reloading paths. Illustration of the hysteretic response of a single nonlinear spring is provided in a later section (Fig. 15).

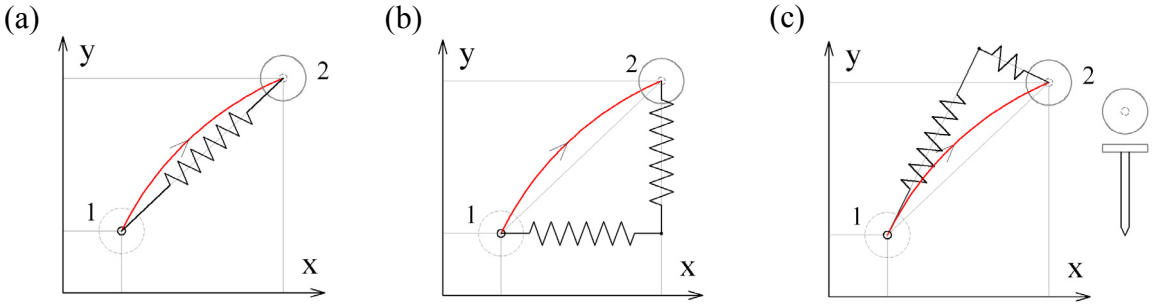

Figure 11: Modeling of a sheathing-to-framing connection using (a) a single spring, (b) a pair of orthogonal springs oriented with the GCS, and (c) a pair of orthogonal springs oriented with the first trajectory of the orbit

4.4 Contact element

A nonlinear elastic contact element is introduced to model bearing (contact) and separation between framing members as well as between horizontal plates and diaphragms. A contact element connects two DOF, oriented at the same direction in the 2D wall plane. Figure 12 illustrates the force-displacement response of the contact spring, while (18) shows the nonlinear mathematical formulation. The variables d_{TOL} and f_{TOL} in (18) are positive real values that are selected as such to be small enough to be considered close to zero, as shown in (19). Thus, the proposed contact element can effectively simulate conditions of absolute contact, while it can be used in parallel or in series with other nonlinear springs to simulate connections between detaching framing members.

$$\mathbf{F_{CON}} = \begin{cases} f_{TOL} \cdot \left(\dfrac{-d_{TOL}}{\mathbf{D_{CON}} + d_{TOL}} + 1 \right), \mathbf{D_{CON}} \geq -0.99 \cdot d_{TOL} \\ -99 \cdot f_{TOL} + 10e04 \cdot \dfrac{f_{TOL}}{d_{TOL}} \cdot \left(\mathbf{D_{CON}} - 0.99 \cdot d_{TOL} \right), \mathbf{D_{CON}} < -0.99 \cdot d_{TOL} \end{cases} \quad (18)$$

$$\text{and } \left((d_{TOL}, f_{TOL}) > 0 \right) \cup \left((d_{TOL}, f_{TOL}) \approx 0 \right) \quad (19)$$

4.5 Modeling of wood framing

When ignoring vertical nonlinearity in the wood framing, the sill (base) plate is fixed to the ground and the framing-to-framing connectors between vertical and horizontal members provide a pinned connection. Gravity loads are applied at the nodes of the top plate that belong to the vertical studs, while the horizontal DOF of the top plate undergo the same displacement, equal to the wall inter-story drift.

When accounting for vertical nonlinearity in the wood framing, the numerical model is formulated as shown in Figure 13. The main feature, in this case, is the duplication of nodes at the top and sill plates to enable modeling of contact/separation phenomena. Contact elements are introduced along vertical DOF at framing-to-framing connections, as well as at the intersection of the sill plate with the ground. Horizontal DOF at framing-to-framing connections are rigidly constrained, while horizontal forces between horizontal plates and diaphragms are transferred through master nodes assigned at the middle of each independent sill or top plate. This enables modeling of the uplifting response without introducing unrealistically high catenary action due to consideration of geometric nonlinearity. This formulation also enables modeling of anchoring devices by introducing springs that connect corresponding vertical DOF of the framing with the ground, as shown in Fig. 13.

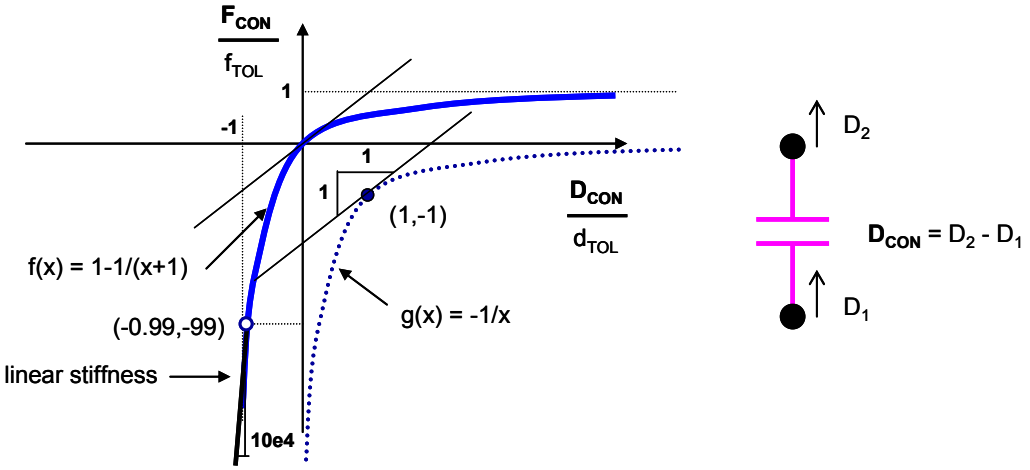

Figure 12: Force-displacement response of a contact element

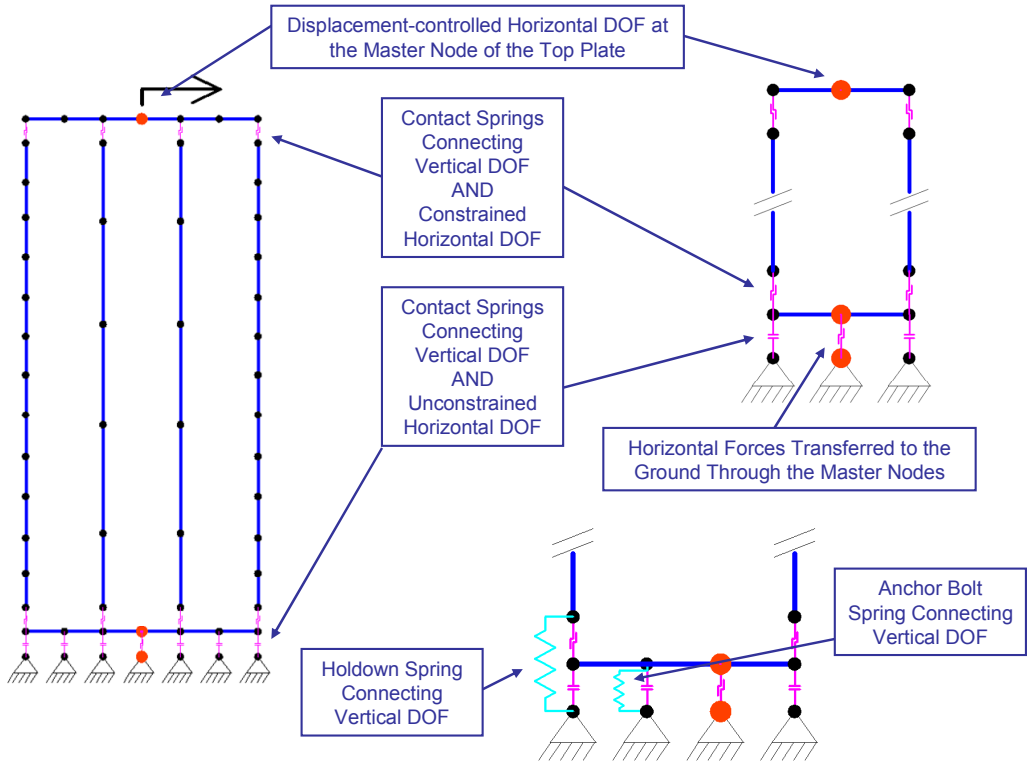

Figure 13: Modeling of wood framing accounting for vertical nonlinearity

4.6 Descriptive summary of the solution algorithm

A Newton-Raphson iterative multi-step procedure, which drives the load imbalance between external and internal forces to zero, is used to solve the nonlinear static equilibrium equations of a single-story multi-panel wall assembly. The tangent global stiffness matrix is updated at all iterations executed within each solution step. Convergence is satisfied when the absolute maximum load imbalance of all the DOF is less than a specified tolerance. A general description of the adopted procedure can be found in [31].

5 EXAMPLE APPLICATION: MONOTONIC & CYCLIC PUSHOVER ANALYSES

This section presents the results obtained from monotonic and cyclic pushover analyses of two segmented[3] shear walls with different aspect ratios. These preliminary analyses serve as a means of demonstrating the features and capabilities of the proposed numerical model.

5.1 Geometry and material properties of two segmented shear walls

Figure 14 illustrates the geometry of the segmented shear walls considered in this example. **ExL** stands for an example shear wall with low aspect ratio, while **ExH** stands for an example shear wall with high aspect ratio. Both segmented shear walls are constructed of identical components and feature the same nailing schedule. Anchoring devices – anchor bolts and holdowns – are installed at the base of the walls. Table 1 contains information on physical dimensions and material properties of the components of the shear walls investigated, while Table 2 presents relevant design calculations. Table 3 summarizes basic properties of the springs used in the numerical analysis. It is interesting to note that the Allowable Stress Design (ASD) capacity of **ExH** is reduced by 40%, as specified by recent design standards, due to the fact that the aspect ratio exceeds a value of 2. This reduction has not been accounted for when calculating the design uplifting force, following intuitive capacity design principles. Furthermore, the vertical response of holdowns and anchor bolts at this preliminary stage of development of the model is assumed to be linear. Finally, Figure 15 illustrates the response of a single sheathing-to-framing connection spring under monotonic and cyclic loading.

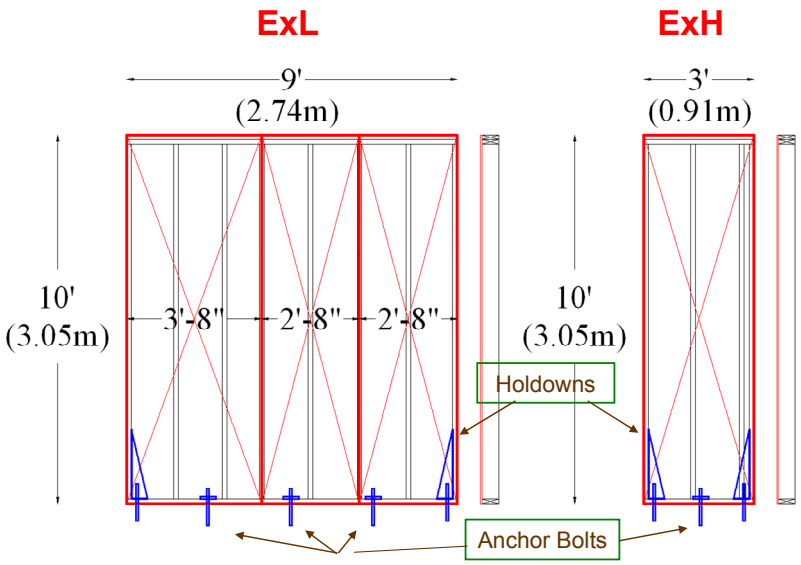

Figure 14: Geometry of example segmented shear walls

[3] Segmented shear wall design considers that only segments of full-height sheathing panels resist lateral loads. Holdown devices are required at the bottom corners of each wall segment to prevent it from overturning.

Table 1: Dimensions and material properties of shear wall components

Wood framing Hem Fir lumber	**Cross section dimensions**	**Modulus of elasticity**
	2" x 6" (nominal)	1.74·E06 psi
	38 x 144 mm	1.20·E07 kPa
Sheathing panel Oriented Strand Board (OSB)	**Thickness**	**Shear modulus**
	7/16"	2.00·E05 psi
	11 mm	1.38·E06 kPa
Sheathing-to-framing connectors 8d common nails	**Length**	**Diameter**
	2.5"	0.131"
	64 mm	3.3 mm

Table 2: Design parameters for investigated shear walls

Abbreviation	**ExL**	**ExH**
Aspect ratio	10/9 = 1.11	10/3 = 3.33
Nailing schedule	Edge/Field Nailing @ 6" / 12" on center	
	Edge/Field Nailing @ 150 mm / 300 mm on center	
ASD capacity (force per length)	260 plf	
	3.8 kN/m	
Aspect ratio adjustment factor	1	2·3/10 = 0.6
ASD capacity (force - including aspect ratio adjustment factor)	260·9·1 = 2340 lbs	260·3·0.6 = 468 lbs
	10.4 kN	2.1 kN
Uplifting design force	260·10 = 2600 lbs	
	11.5 kN	11.5 kN

Table 3: Spring properties used in analyses

Sheathing -to- framing connection spring	**Initial stiffness**	**Capping force**	**Displacement at capping force**	**Displacement at failure**
	6645 lbs/in	316 lbs	0.5"	2.5"
	1.16 kN/mm	1.4 kN	12.7 mm	63.5 mm
Contact spring	**f_{TOL}**	**d_{TOL}**	**Holdown and Anchor Bolt springs**	**Stiffness ***
	3.1 lbs	7.5·E-04"		32700 lbs/in
	1.4·E-02 kN	1.9·E-02 mm		5.70 kN/mm

* Stiffness of linear springs for holdowns estimated as the ratio of the allowable force (3270 lbs) over the displacement at the allowable force (0.1") as given by the manufacturer for holdown PHD5-SDS3. Stiffness of linear springs for anchor bolts was selected equal to the stiffness of holdowns at this preliminary stage.

5.2 Analysis cases

Three analysis cases have been considered in this study. These are:

1) **Uplift Off**: No vertical separation of sill plate from the ground. Pinned stud-to-plate framing connections;

2) **Uplift On**: Consideration of vertical separation between framing members and diaphragms. Consideration of holdowns and anchor bolts;
3) **No HDs**: Similar to **Uplift On** excluding the inclusion of holdowns in the numerical model.

Furthermore, the effect of the amplitude of gravity loads has been investigated, considering various amplitudes of distributed gravity forces.

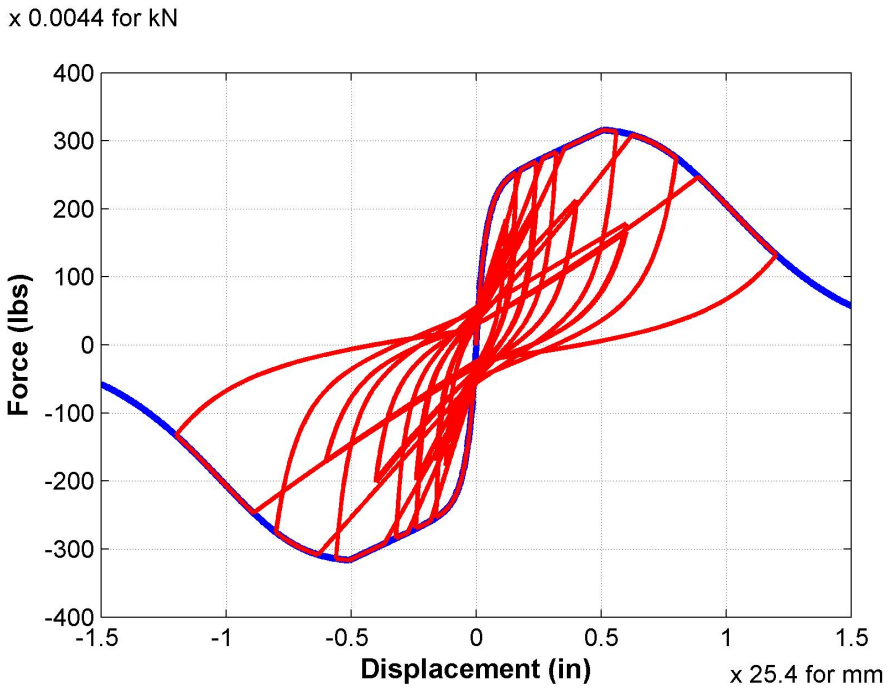

Figure 15: Monotonic and cyclic response of a single sheathing-to-framing connection spring

5.3 Monotonic pushover analysis results

Figures 16a and 16b present the monotonic pushover analysis results for the first two analysis cases (**Uplift Off - Uplift On**), featuring three amplitudes of the distributed gravity forces. For the analysis case where uplifting behavior is neglected, it can be observed that the variation of the gravity load has no significant effect on the load-deformation characteristics. As expected, increasing gravity forces results in lower capping force, achieved at lower wall inter-story drifts, but the stiffness and force at low displacement amplitudes is not modified. This is also depicted in Fig.17a, which illustrates the variation of capping force for each monotonic analysis conducted.

When vertical nonlinearity in the framing is considered (**Uplift On**), it is observed that there is a reduction of the initial as well as the effective stiffness throughout the wall deformation range. Increasing gravity forces results in an increase of the initial stiffness, as well, contrary to what observed in the first analysis case. Fig. 17a illustrates that, when increasing gravity forces, the capping force, as well as the wall drift at maximum force, increases up to a certain point, after which a reduction in both magnitudes is observed. These phenomena are more identifiable in the wall with high aspect ratio, indicating a first sign of the susceptibility of walls with similar aspect ratios to reduced global resistance.

Fig. 17b illustrates the maximum uplifting forces developed in the holdowns and anchor bolts. As shown in Fig. 17b, the magnitude of uplifting forces is similar for both example

shear walls, while the forces developed in holdowns exceed the ASD values, ranging close to ultimate resistance values.

5.4 Cyclic pushover analysis results

Figures 18 and 19 illustrate the cyclic analysis pushover results for **ExL** and **ExH**, respectively. Cyclic analyses have been performed for all 3 analysis cases; for a single gravitational distributed load (1.2 klf), which produced the highest capping force in monotonic analyses.

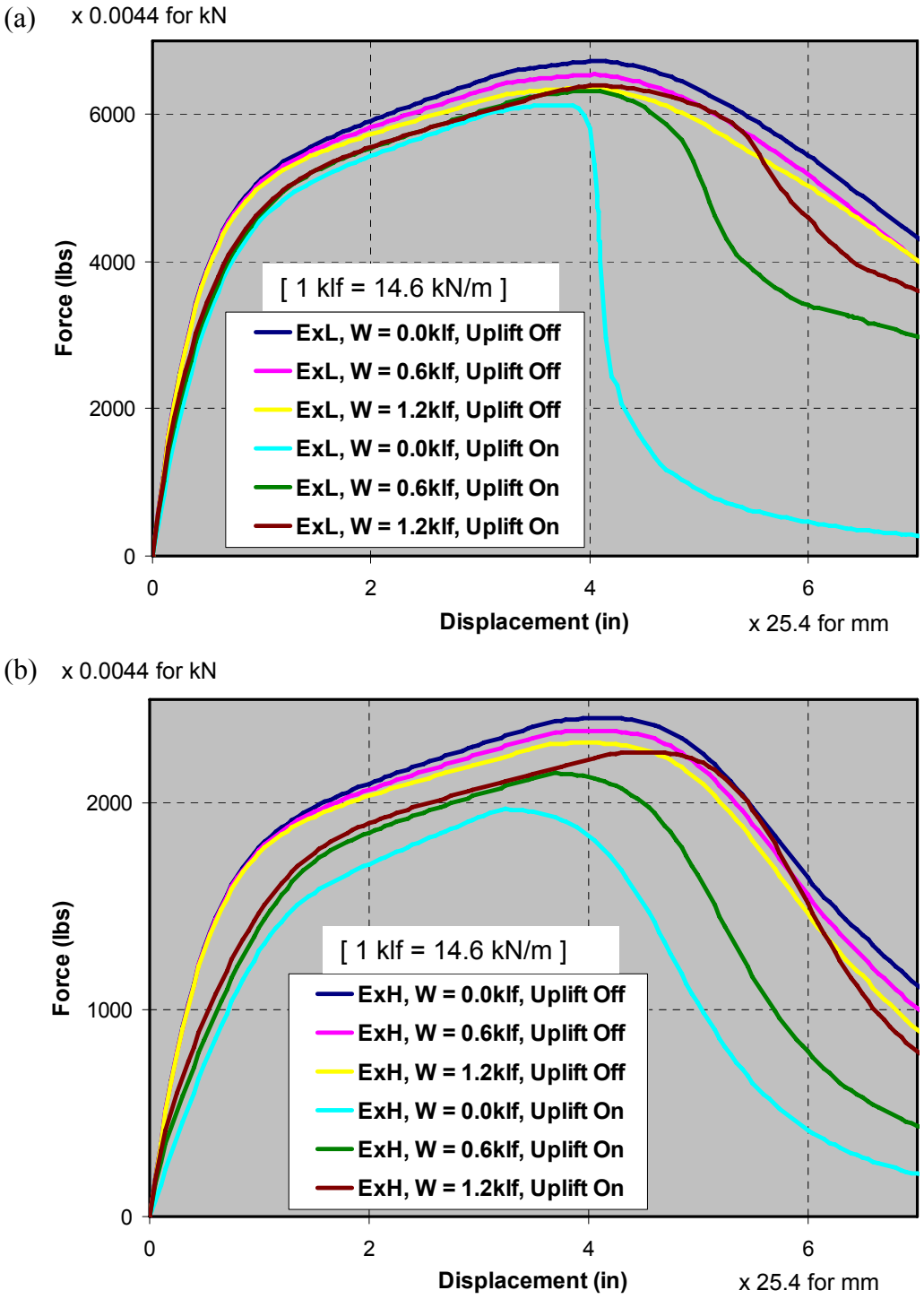

Figure 16: Results of pushover monotonic analysis for (a) **ExL**, and (b) **ExH**

For the example shear wall with low aspect ratio (**ExL**), it is observed that the consideration of vertical nonlinearity in the framing results in a reduction of the dissipated strain energy of the order of 5-10%. When holdowns are not introduced, the wall resistance drops significantly, resulting in a reduction of the dissipated energy by 30-40%.

For the example shear wall with high aspect ratio (**ExH**), it is observed that the consideration of vertical nonlinearity in the framing results in a reduction of the dissipated strain energy of the order of 20-30%. When holdowns are not introduced, a rocking response can be identified – characterized as "flag-shaped" – with minimal residual deformations and reduced energy dissipation by more than 80%.

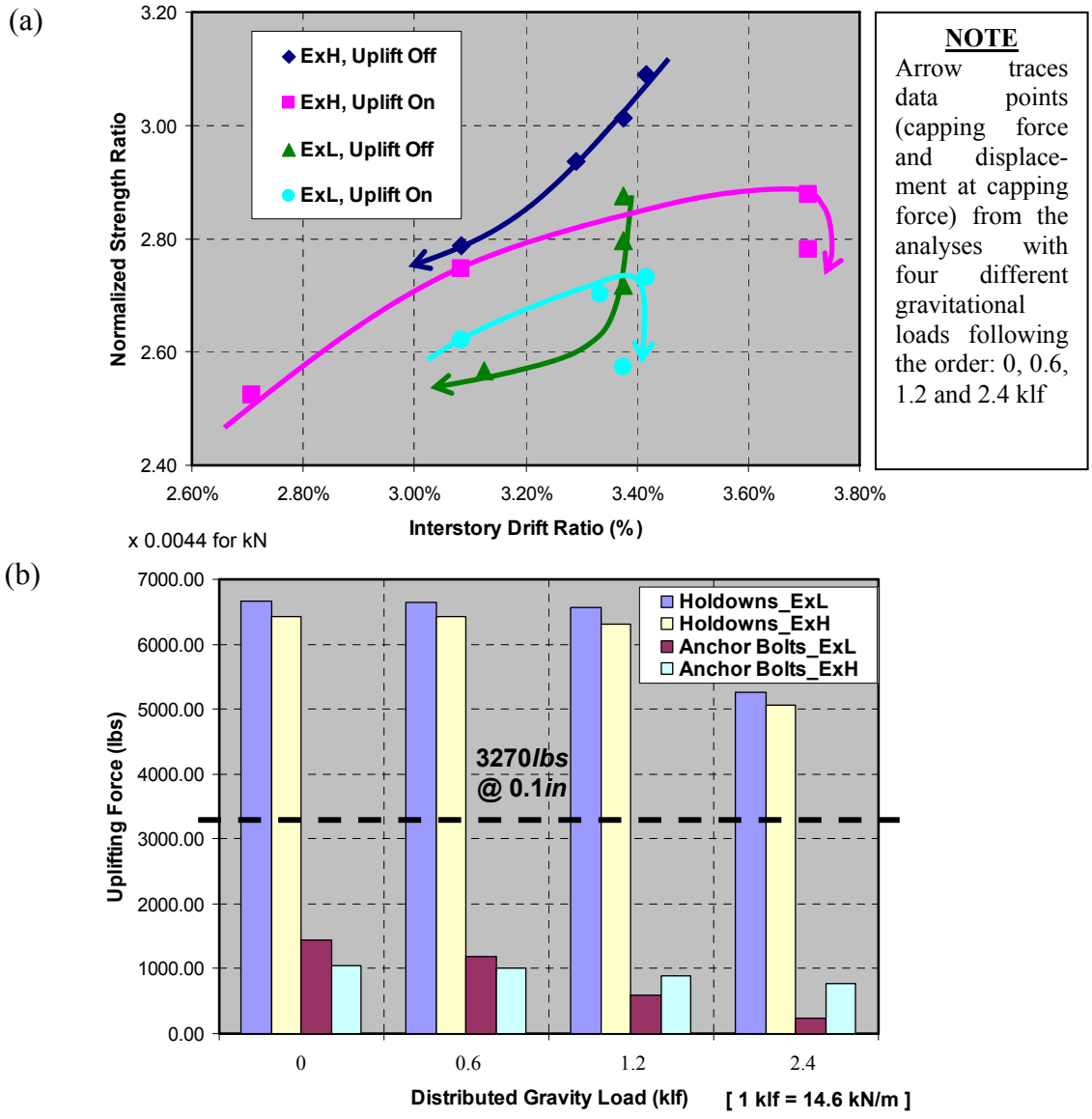

Figure 17: Additional results from monotonic pushover analysis; (a) variation of capping force, and (b) maximum uplifting forces

6 CONCLUSIONS AND FUTURE WORK

The monotonic and cyclic pushover analysis results have demonstrated the capability of the proposed numerical model to capture the differences in stiffness, strength and overall hysteretic behavior of two single-story multi-panel segmented shear walls with different aspect

ratios, constructed with different anchorage conditions (full anchorage – analysis case 2 – and partial anchorage – analysis case 3). The wall with high aspect ratio has been found to be more susceptible to a rocking mode of deformation than the wall with low aspect ratio.

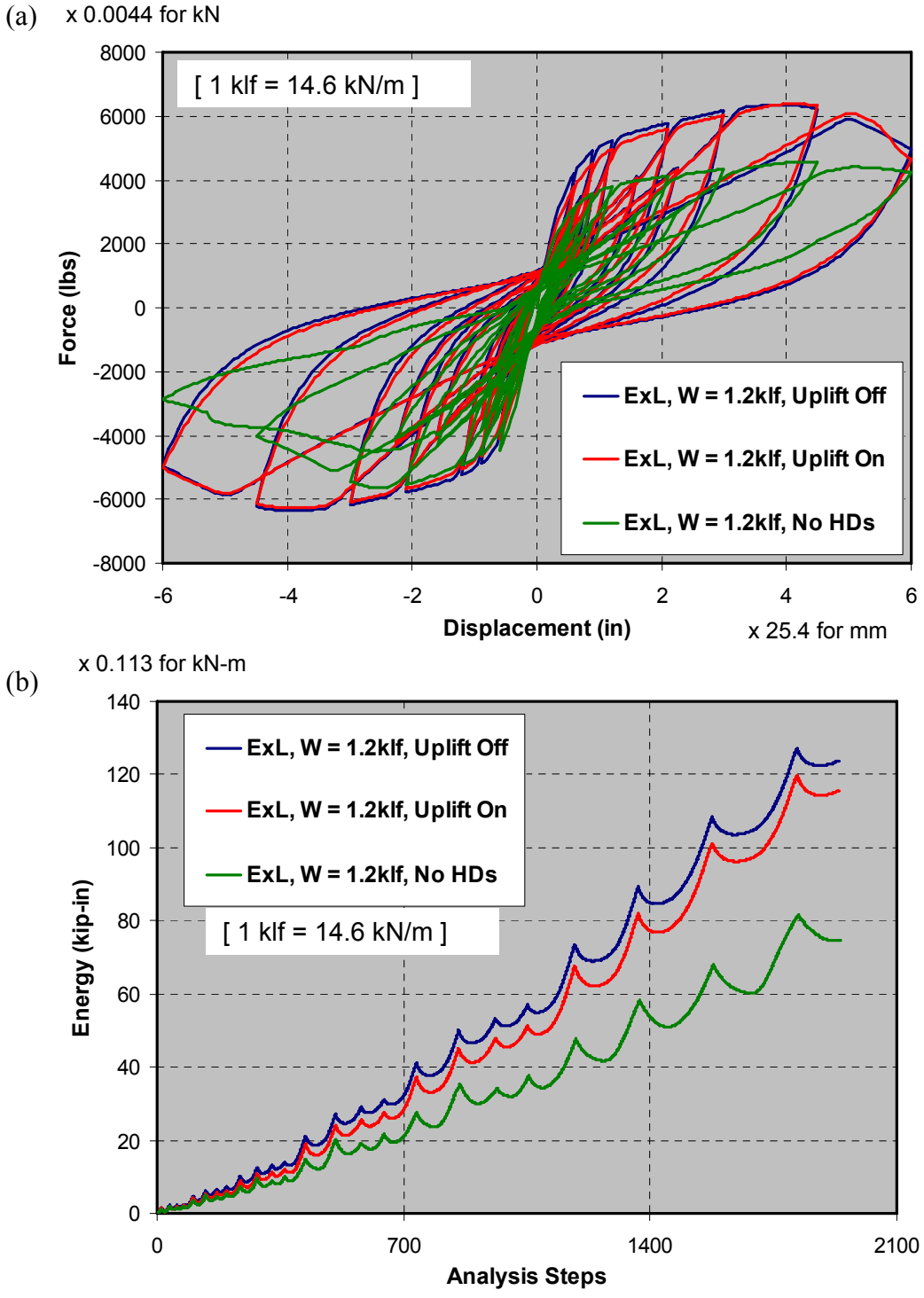

Figure 18: Results of pushover cyclic analysis for **ExL**; (a) force-displacement curve, and (b) strain energy

The neglection of contact/separation and uplifting response leads to unconservative estimates of the energy dissipation capability under cyclic loading. Thus, it is important to consider these effects, especially for seismic collapse assessment studies, since the energy

dissipation capability affects fundamentally the collapse capacity of structural systems under earthquake shaking.

Future work focuses on integrating the proposed shear wall model to a 2D multi-story numerical building model to be used for static and dynamic analysis [34].

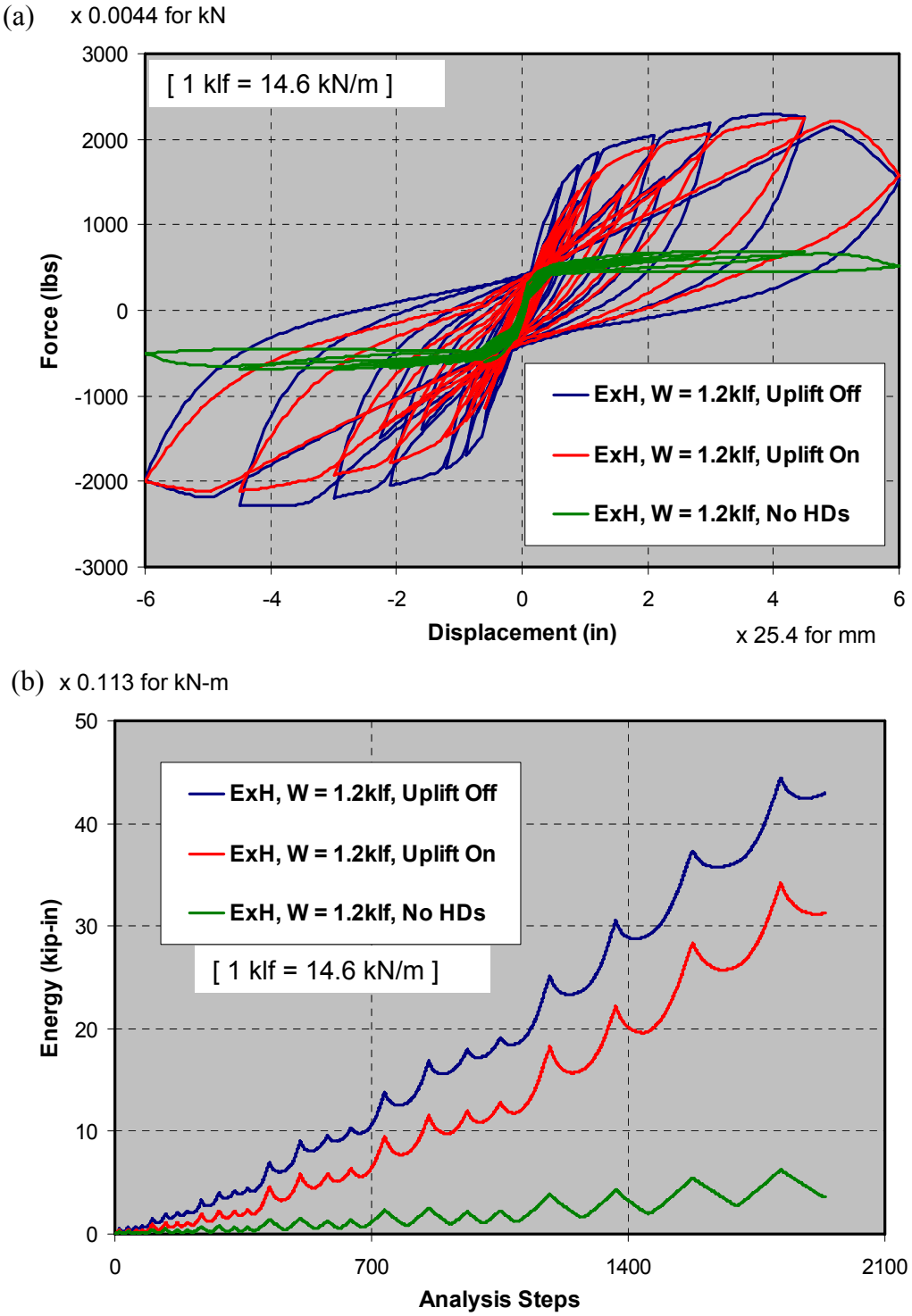

Figure 19: Results of pushover cyclic analysis for **ExH**; (a) force-displacement curve, and (b) strain energy

ACKNOWLEDGEMENTS

The authors would like to thank Prof. W.C. Pang from Clemson University for providing the subroutine used to model the sheathing-to-framing connections. The material presented in this paper is based upon work supported by the National Science Foundation under Grant No. CMMI-0529903 (NEES Research) and CMMI-0402490 (NEES Operations). Any opinions, findings, and conclusions or recommendations expressed in this material are those of the author(s) and do not necessarily reflect the views of the National Science Foundation.

REFERENCES

[1] CUREe, 1998. CUREe-Caltech Woodframe Project Newsletter, Issue No. 1, available online at http://www.curee.org/projects/woodframe/.

[2] Ekiert, C. and Hong, J. 2006. "Framing-to-Sheathing Connection Tests in Support of NEESWood Project," Network of Earthquake Engineering Simulation Host Institution: State University of New York at University at Buffalo, Buffalo, NY. 20 p.

[3] Pardoen, G.C., Walman, A., Kazanjy, R.P., Freund, E. and Hamilton, C.H., 2003. "Testing and Analysis of One-Story and Two-Story Shear Walls Under Cyclic Loading," CUREe Publication No. W-25, CUREE-Caltech Woodframe Project.

[4] Falk, R.H. and Soltis, L.A., 1988. "Seismic Behavior of Low-Rise Wood-Framed Buildings," *The Shock and Vibration Digest,* **20**(12):3-7.

[5] EQE International and the Governor's Office of Emergency Services, 1995. The Northridge Earthquake of January 17, 1994: Report of Data Collection and Analysis, Part A, p. 5-18 (Sacramento, CA: Office of Emergency Services).

[6] Hall, J.F. (Primary Contributor), Schmid, B., Comerio, M. and Russell, J., 1996. "Northridge Earthquake of January 17 1994 Reconnaissance Report Volume 2: Wood Buildings," *Earthquake Spectra,* **12**(S1):125-176.

[7] Perkins, J.B., Boatwright, J. and Chaqui, B., 1998. Housing Damage and Resulting Shelter Needs: Model Testing and Refinement Using Northridge Data, Proceedings of the NEHRP Conference and Workshop on Research on the Northridge, California Earthquake of January 17, 1994, Vol. IV (Richmond, CA: California Universities for Research in Earthquake Engineering).

[8] Kircher, C.A., Reitherman, R.K., Whitman, R.V. and Arnold, C., 1997. "Estimation of Earthquake Losses to Buildings," *Earthquake Spectra,* **13**(4).

[9] USGS, 2009. U.S. Geological Survey website, available online at http://www.usgs.gov/.

[10] Folz, B. and Filiatrault, A., 2001. "Cyclic Analysis of Wood Shear Walls," *Journal of Structural Engineering,* ASCE, **127**(4):433-441.

[11] Folz, B. and Filiatrault, A., 2004a. "Seismic Analysis of Woodframe Structures I: Model Formulation," *Journal of Structural Engineering,* ASCE, **130**(9):1353-1360.

[12] Folz, B. and Filiatrault, A., 2004b. "Seismic Analysis of Woodframe Structures II: Model Implementation and Verification," *Journal of Structural Engineering,* ASCE, **130**(9):1361-1370.

[13] Christovasilis, I.P., Filiatrault, A., Wanitkorkul, A. and Constantinou, M.C., 2008. "Incremental Dynamic Analysis of Woodframe Buildings", *Journal of Earthquake Engineering and Structural Dynamics* (online publication), John Wiley & Sons, Ltd.

[14] FEMA, 2008. "Quantification of building seismic performance factors." ATC-63 Project Report - 90% Draft, FEMA P695, Applied Technology Council, Redwood City, CA.

[15] Ayoub, A., 2007. "Seismic Analysis of Wood Building Structures," *Engineering Structures,* **29**:213-223.

[16] Judd, J.P., 2005. "Analytical Modeling of Wood-Frame Shear Walls and Diaphragms," M.Sc. Thesis, Department of Civil and Environmental Engineering, Brigham Young University, Provo, Utah.

[17] He, M., Lam, F. and Foschi, R.O., 2001. "Modeling Three-Dimensional Timber Light-Frame Buildings," *Journal of Structural Engineering,* ASCE, **127**(8):901-913.

[18] White, M.W. and Dolan, J.D., 1995. "Nonlinear Shear-Wall Analysis," *Journal of Structural Engineering,* ASCE, **121**(11):1629-1635.

[19] Collins, M., Kasal, B., Paevere, P.J. and Foliente, G.C., 2005a. "Three-Dimensional Model of Light Frame Wood Buildings. I: Model Description," *Journal of Structural Engineering,* ASCE, **131**(4):676-683.

[20] Collins, M., Kasal, B., Paevere, P.J. and Foliente, G.C., 2005b. "Three-Dimensional Model of Light Frame Wood Buildings. I: Experimental Investigation and Validation of Analytical Model," *Journal of Structural Engineering,* ASCE, **131**(4):684-692.

[21] Dujic, B. and Zarnic, R., 2004. "Method for Modelling Dynamic Response of Timber Frame Building," *Proceedings of the 8th World Conference on Timber Engineering*, Lahti, Finland.

[22] Ceccotti, A., Follesa, M. and Karacabeyli, E., 2000. "3D Seismic Analysis of Multi-Storey Wood Frame Construction", *Proceedings of the 6th World Conference on Timber Engineering,* British Columbia, Canada.

[23] Andreasson, S., 2000. "Three-Dimensional Interaction in Stabilization of Multi-Storey Timber Frame Building Systems," Ph.D. Thesis, Division of Structural Engineering, Lund University, Lund, Sweden.

[24] Tarabia, A.M. and Itani, R.Y., 1997. "Seismic Response of Light-Frame Wood Buildings," *Journal of Structural Engineering,* ASCE, **123**(11):1470-1477.

[25] Xu, J., 2006. "Development of a General Dynamic Hysteretic Light-Frame Structure Model and Study on the Torsional Behavior of Open-Front Light-Frame Structures," Ph.D. Thesis, Department of Civil and Environmental Engineering, Washington State University, Pullman, Washington.

[26] Schmid, B.L., Nielse, R.J. and Linderman, R.R., 1994. "Narrow Plywood Shear Panels," *Earthquake Spectra,* **10**(3):569-588.

[27] Dolan, J.D. and Johnson, A.C., 1997. "Monotonic Tests of Long Shear Walls with Openings," Department of Wood Science and Forests Products, Report No. TE-1996-001, Virginia Polytechnic Institute and State University, Blacksburg, Virginia.

[28] Salenikovich, A.J., 2000. "The Racking Performance of Light-Frame Shear Walls," Ph.D. Thesis, Department of Wood Science and Forest Products, Virginia Polytechnic Institute and State University, Blacksburg, Virginia.

[29] Fischer, D., Filiatrault, A., Folz, B., Uang, C.M. and Seible, F., 2001. "Shake Table Tests of a Two-Story Woodframe House," CUREe Publication No. W-06, CUREE-Caltech Woodframe Project.

[30] Christovasilis, I.P., Filiatrault, A. and Wanitkorkul, A., 2007. "Seismic Testing of a Full-Scale Two-Story Light-Frame Wood Building: NEESWood Benchmark Test," NEESWood Report No. NW-01, Department of Civil, Structural and Environmental Engineering, University at Buffalo, State University of New York, Buffalo, New York.

[31] Cook, R.D., Malkus, D.S., Plesha, M.E. and Witt, R.J., 2002. "Concepts and Applications of Finite Element Analysis," 4th Edition, John Wiley & Sons, Ltd.

[32] Judd, J.P. and Fonseca, F.S., 2005. "Analytical Model for Sheathing-to-Framing Connections in Wood Shear Walls and Diaphragms," *Journal of Structural Engineering,* ASCE, **131**(2):345-352.

[33] Pang, W.C., Rosowsky, D.V., Pei, S. and van de Lindt, J.W., 2007. "Evolutionay Parameter Hysteretic Model for Wood Shear Walls," *Journal of Structural Engineering,* ASCE, **133**(8):1118-1129.

[34] Christovasilis, I.P., 2009. "Numerical and Experimental Investigations of the Seismic Response of Light-Frame Wood Structures," Ph.D. Thesis, Department of Civil, Structural and Environmental Engineering, University at Buffalo, State University of New York, Buffalo, New York, (available September 2009).